ADVANCED HEALTHCARE MATERIALS
www.advhealthmat.de

Programmable Delivery of Synergistic Cancer Drug Combinations Using Bicompartmental Nanoparticles

Jason V. Gregory, Douglas R. Vogus, Alexandra Barajas, Melissa A. Cadena, Samir Mitragotri, and Joerg Lahann**

Delivery of multiple therapeutics has become a preferred method of treating cancer, albeit differences in the biodistribution and pharmacokinetic profiles of individual drugs pose challenges in effectively delivering synergistic drug combinations to and at the tumor site. Here, bicompartmental Janus nanoparticles comprised of domains are reported with distinct bulk properties that allow for independent drug loading and release. Programmable drug release can be triggered by a change in the pH value and depends upon the bulk properties of the polymers used in the respective compartments, rather than the molecular structures of the active agents. Bicompartmental nanoparticles delivering a synergistic combination of lapatinib and paclitaxel result in increased activity against HER2+ breast cancer cells. Surprisingly, the dual drug loaded particles also show significant efficacy toward triple negative breast cancer, even though this cancer model is unresponsive to lapatinib alone. The broad versatility of the nanoparticle platform allows for rapid exploration of a wide range of drug combinations where both their relative drug ratios and temporal release profiles can be optimized.

1. Introduction

Cancer therapeutics are most effective, when administered in combination with one another due to tumor heterogeneity and acquired resistance mechanisms. Combination therapy, an approach of administering two or more therapeutic agents or treatment modalities, is thus increasingly applied in cancer therapy.[1] In contrast to single drugs, the administration of multiple therapeutics has the advantage that several pathways contributing to cell survival and proliferation, apoptosis, and metastatic behavior can be targeted simultaneously. The approach of targeting orthogonal pathways offers the benefit of achieving greater therapeutic effects, while also reducing the individually required doses and associated off-target side effects, blocking of prosurvival pathways, and minimizing the occurrence of drug resistance often observed in patients.[1–4] As a result, extensive research has been conducted to identify and optimize synergistic drug combinations.[5–9] Critical challenges include the effective delivery of identified combinations, in part due to ineffective means to control the biodistribution and pharmacokinetics of the individual agents. Additionally, it has been observed in some cases that optimal synergistic effects are dependent not only on the precise control over the molar ratios delivered but also on the sequence in which the two drugs are administered.[10]

A wide range of polymer nanoparticles have been extensively developed for the use as drug carriers.[11–13] Previous work has demonstrated electrohydrodynamic (EHD) cojetting as a versatile and highly scalable means to synthesize multicompartmental micro- and nanoparticles.[14,15] Bicompartmental particles have previously been engineered to carry small molecule drugs,[16,17] siRNA,[18,19] and imaging agents for various therapeutic applications.[20] In addition, bicompartmental particles can be synthesized at sizes less than 200 nm and selectively surface modified with functional ligands.[21–23] Downstream processing, including surface PEGylation,[21] CD-47 presentation,[24,25] and red blood cell (RBC) hitchhiking,[26] are each possible alone or in combination using these nanoparticles and can be leveraged to alter biodistribution of particles. Contrary to other nanoparticle fabrication methods, bicompartmental nanoparticles formed via EHD cojetting allow for individual drugs to be loaded into distinct compartments, comprising of unique materials, capable of degrading at different rates, and thereby resulting in distinct and controlled release kinetics.[27,28]

J. V. Gregory, Prof. J. Lahann
Biointerfaces Institute and Department of Chemical Engineering
University of Michigan
Ann Arbor, MI 48109, USA
E-mail: lahann@umich.edu
Dr. D. R. Vogus, Prof. S. Mitragotri
John A Paulson School of Engineering and Applied Sciences
Harvard University
Cambridge, MA 02138, USA
E-mail: mitragotri@seas.harvard.edu
A. Barajas
Department of Chemical Engineering
University of California, Santa Barbara
Santa Barbara, CA 93106, USA
M. A. Cadena, Prof. J. Lahann
Department of Biomedical Engineering
University of Michigan
Ann Arbor, MI 48109, USA
The ORCID identification number(s) for the author(s) of this article can be found under https://doi.org/10.1002/adhm.202000564

DOI: 10.1002/adhm.202000564

 © 2020 Wiley-VCH GmbH

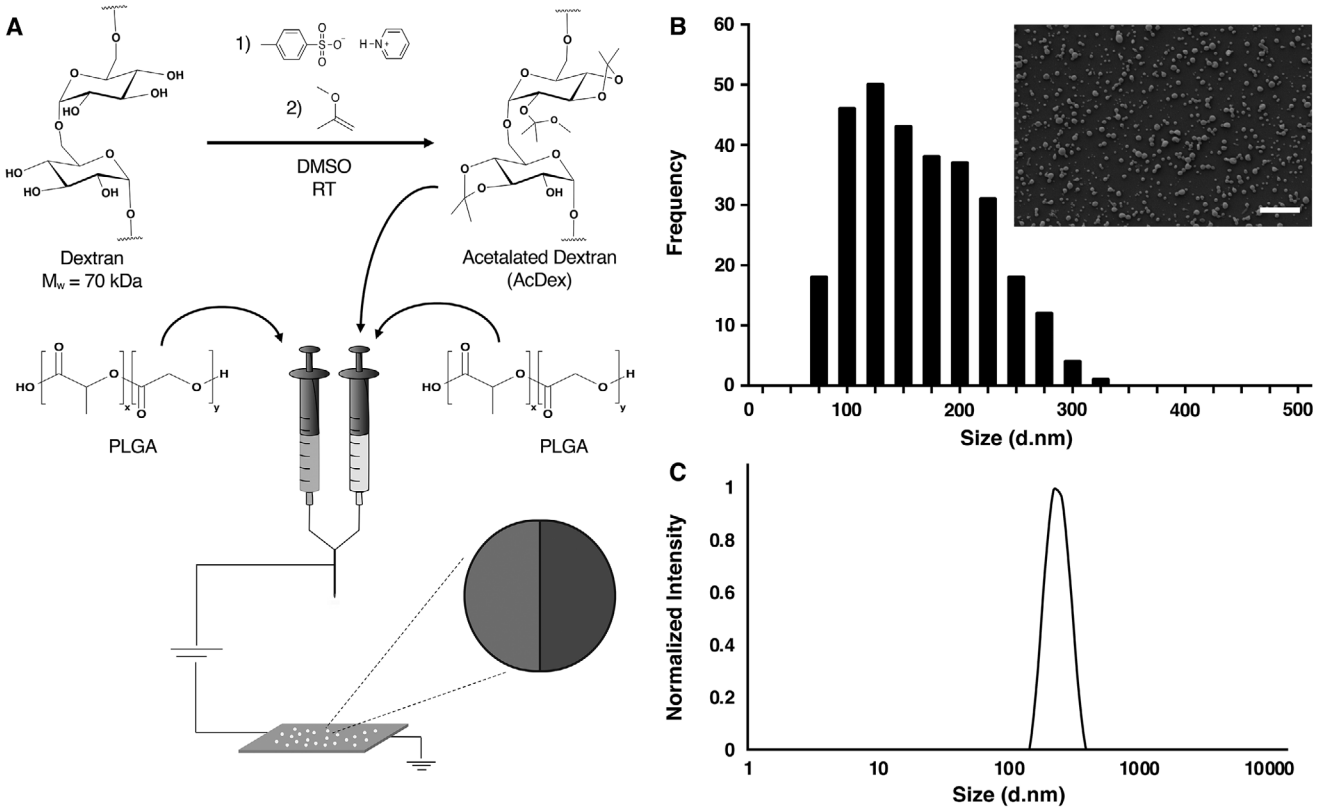

Figure 1. Synthesis of bicompartmental nanoparticles via EHD cojetting. A) Reaction scheme for the chemical synthesis of pH responsive, acetalated dextran (AcDex) and incorporation of the resulting polymer to produce bicompartmental nanoparticles. B) Representative SEM image (inset) and size distribution of cojetted bicompartmental nanoparticles. Average diameter = 161 ± 61.2 nm. Scale bar = 1 μm. C) Dynamic light scattering (DLS) size characterization of bicompartmental nanoparticles in PBS. Average diameter = 240 nm.

This research aims to develop a single nanoparticle platform from which the controlled release of two distinct therapeutics can be achieved, independent of their chemical/biological properties. In particular, we seek to engineer programmable nanoparticles with tunable drug ratios and decoupled release kinetics.

2. Results

2.1. Bicompartmental Nanoparticle Synthesis and Characterization

Taking advantage of the biological difference in pH, typical of tumor microenvironments (TME), and endocytotic cellular compartments (i.e., endosomes and lysosomes), we aimed to engineer bicompartmental nanoparticles that would preferentially degrade in acidic conditions. Previous work by Fréchet and coworkers resulted in the synthesis of an acetal-modified dextran (AcDex) by reacting hydroxyl groups with 2-methoxypropene.[29] Acetylated dextran was explored previously as a material compatible with electrohydrodynamic jetting through the formation of fibrous scaffolds and nanoparticles.[30,31] Following a similar synthetic route, we modified a 70 kDa dextran to ensure that resulting polymer is no longer readily water soluble and the protecting groups impart more hydrophobic properties. Under acidic conditions, the acetal groups are readily cleaved resulting in the release of methanol and acetone moieties and a return to the water-soluble dextran structure. Combined with poly(lactic-*co*-glycolic acid) (PLGA) within a single nanoparticle (**Figure 1**A), the result is a bicompartmental particle with distinct degradation rates in response to pH.

Prior to the fabrication of drug-loaded bicompartmental nanoparticles, synthesized AcDex was first validated through ^{1}H NMR spectroscopy and particle degradation experiments. Together with a noticeable change in solubility, initial NMR spectra (^{1}H, $CDCl_3$, Figure S1, Supporting Information), when compared to literature describing the synthesis of low molecular weight (10 kDa) AcDex,[29] confirmed polymer structure. Following polymer degradation via hydrolysis in D_2O/DCl, chemically cleaved protecting groups yield acetone and methanol, each detectable via ^{1}H NMR at ≈2.2 and 3.3 ppm, respectively. In the case of acyclic protecting groups, both acetone and methanol are produced; conversely, cyclic protecting groups yield only acetone. Integration of the resulting methanol and acetone NMR peaks suggested that ≈70% of the available dextran hydroxyl groups were protected, rendering the resulting polymer insoluble in neutral aqueous conditions (Figure S1, Supporting Information). Further examination of the same spectra indicated that the ratio of hydroxyls protected by acyclic to cyclic acetal groups was ≈4:1 (Figure S1, Supporting Information). Previous studies suggest that this approaches the maximum achievable ratio of cyclic protecting groups due to the chemical structure of dextran and

© 2020 Wiley-VCH GmbH

hydroxyl groups available to participate in such bonding. The ratio of acyclic to cyclic protecting groups is easily modified through reaction conditions and ultimately contributes to particle degradation rates.[32]

To further characterize the synthesized AcDex polymer, multicompartmental nanoparticles consisting of a PLGA and PLGA/AcDex compartments were fabricated via EHD cojetting (Figure 1A). EHD cojetting utilizes the laminar flow of two or more polymer solutions, in specific geometric arrangements, to produce bicompartmental particles with anisotropic bulk and surface properties. The application of an electric field to the compound droplet results in the formation of a Taylor cone and electrified polymer jet. Acceleration of the viscoelastic jet in the electric field leads to the reduction in thread diameter by several orders of magnitude facilitating rapid solvent evaporation and solidification of nonvolatile components. In the absence of convective mixing at the stable droplet interface, the resulting particle geometry is reflective of the original droplet orientation. Capable of incorporating a wide range of materials, the EHD cojetting process permits the synthesis of particles with several substantially dissimilar and decoupled compartments, including the encapsulation of imaging or therapeutics modalities.[16–18,31]

The resulting spherical nanoparticles, when imaged using scanning electron microscopy (SEM), were found to be relatively homogeneous in size with an average diameter in their dry state of 161 ± 61.2 nm (Figure 1B). This technique allowed for both the surface morphology to be examined while simultaneously determining a statistically significant size distribution. Once collected and purified, their average hydrodynamic diameter, measured by dynamic light scattering (DLS), was determined to be 240 nm, Polydispersity Index (PDI) = 0.316 (Figure 1C). The discrepancy in size can be attributed to a combination of swelling of the polymer nanoparticles in solution and inherent differences in the measurement techniques. When additional purification was performed through centrifugation methods we were able to obtain fractions of smaller particles, ≈175 nm (PDI = 0.174) in diameter as measured by DLS (Figure S2, Supporting Information). Particles were then incubated in either neutral or acidic buffer at 37 °C for 5, 10, 15, and 20 h. These particles were then extensively washed, deposited on silicon wafers, and imaged via SEM to visually investigate their degradation in response to pH. It was observed that particles in acidic buffer underwent significant swelling and rapid degradation compared to those incubated in neutral conditions (Figure S3, Supporting Information). This observed difference in nanoparticle degradation would suggest that the acetal protected dextran remains water insoluble under neutral conditions; however, when exposed to acidic environments, the polymer readily undergoes acid catalyzed hydrolysis, is converted back to its water-soluble form, and results in a rapid degradation of the AcDex containing particle hemisphere. Together, these properties offer an ability to tune the release kinetics of encapsulated molecules in response to external stimuli, notably the pH of the surrounding environment.

To demonstrate the difference in degradation of each of the polymer phases and its effect on the release of encapsulated small molecules, Rhodamine B was incorporated into the AcDEX/PLGA compartment while Coumarin was loaded into the PLGA compartment. The addition of dyes to the synthesized nanoparticles did not significantly change the resulting nanoparticles shape or size as confirmed by the respective SEM images (**Figure 2**A). Super resolution, structured illumination microscopy (SIM) of the resulting nanoparticles clearly shows the formation of two distinct compartments, each containing the loaded dye molecules (Figure 2A). The particles were found to have diameters consistent with previous measurements taken in their dry state and imaged using SEM. The release kinetics of each fluorescent molecule at physiologically relevant conditions were determined (Figure 2B–E). Neutral conditions (pH 7.2) were selected to inform release kinetics from particles in circulation and healthy extracellular space while pH 5.0 was evaluated to characterize release in the more acidic TME and endocytotic vesicles. Together, these two conditions were chosen to provide a more complete representation of drug release following systemic delivery. The stability of both polymer phases was evident by the slow release kinetics of the fluorescent molecules at pH 7.2 (Figure 2B). At pH 5, the release of Rhodamine B from the AcDEX/PLGA compartment phase of the nanoparticles is noticeably faster than that of coumarin from the PLGA compartment (Figure 2C). This was also evident after changing the pH of the solution from pH 7.4 to pH 5.0 at $t = 24$ h (Figure 2D). While we observed an obvious divergence of the individual release profiles following the change in pH at 24 h, it was also noted that nearly 75% of each encapsulated material had already been released; experimental designs for subsequent release experiments were adjusted to account for this. Finally, comparing the initial release of Rhodamine B from the acetylated dextran phase in acidic pH, it is clearly more rapid than when the nanoparticles are incubated at neutral pH (Figure 2E).

2.2. Activity in HER2+ Breast Cancer Models

After establishing the ability to both load and release small molecule surrogates from bicompartmental nanoparticles, work was done to identify and optimize a potentially synergistic drug combination. Lapatinib (LAP), a dual epidermal growth factor receptor (EGFR) and human epidermal growth factor receptor 2 (HER2) kinase inhibitor, was originally approved for treating late stage, HER2+ breast cancer in combination with capecitabine. Since then, it has been tested in various clinical trials as a substitute for trastuzumab in combination with other chemotherapeutic agents. In particular, LAP and paclitaxel (PTX) have been evaluated for treatment of various phenotypes of metastatic breast cancer.[33–37] Overexpression of tyrosine-kinase activity is essential in many biological functions, including those contributing to chemoresistance.[38,39] In patients that fail to respond to broadly applied chemotherapeutics such as PTX, inhibiting this pathway has been shown to regain efficacy.[40] Therefore, it has been proposed that the combination of tyrosine-kinase inhibitors with taxanes may prove to be effective treatment regimens. The addition of LAP to PTX chemotherapy regimens has extended the survival of patients with metastatic, HER2+ cancer while being mostly ineffective for HER2- patients.[33,34,36] In addition, LAP and PTX have proven to be effective in treating HER2+ breast cancer patients in the neoadjuvant setting.[37] The use of high doses of LAP

© 2020 Wiley-VCH GmbH

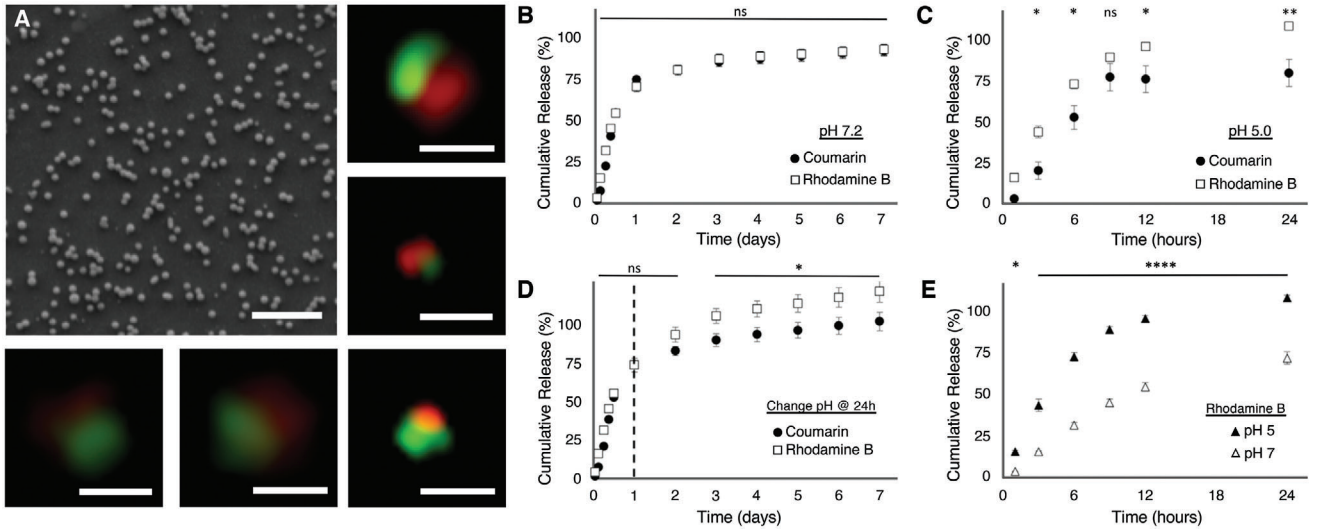

Figure 2. Dye loading and controlled release from bicompartmental PLGA/AcDex nanoparticles. A) SEM image of dye-loaded bicompartmental nanoparticles. Average size = 165 ± 37 nm. Individual particles imaged with super-resolution, structured illumination microscopy (SIM) showing distinct compartments within single particles. Scale bar (SEM) = 1 µm, Scale bars (SIM) = 300 nm. B–E) Release of encapsulated small molecule dyes Coumarin and Rhodamine B from PLGA and pH responsive PLGA/AcDex compartments, respectively. Release kinetics studied at B) physiological pH, 7.2, C) acidic pH, 5.0, and D) a dynamic system with a change of pH from 7.2 to 5.0 at the 24 h timepoint. E) Release kinetics of Rhodamine B, encapsulated within the pH responsive PLGA/AcDex compartment evaluated at both neutral and acidic conditions. Results are shown as mean ± standard deviation (SD). Statistical significance defined as $p < 0.05$ ($n \geq 3$ biological replicates; two-way ANOVA and Sidak's multiple comparisons tests; **** $p < 0.0001$, ** $p < 0.005$, * $p < 0.05$).

has also been used to increase the delivery of albumin bound PTX to various solid tumors by reducing the hyperpermeability of the tumor vasculature.[41] While promising, other studies have found no true synergistic effect between the two drugs when delivered simultaneously.[42]

Given the early, yet conflicting, clinical success of PTX and LAP in combination, it poses the question if the combination's efficacy could be further improved if the drugs are administered in an optimal manner. However, designing the optimal combination regimen for PTX and LAP in their free forms is a challenge due to the drugs being administered through different routes: LAP as an oral pill and PTX intravenously with Cremophor EL. To ensure the drugs reach the tumor site simultaneously, various delivery systems have been synthesized to codeliver the two hydrophobic agents. In particular, LAP and PTX have been loaded into the core of micelles,[40,43–45] liposomes,[46] injectable hydrogels,[47] and layer-by-layer nanoparticles.[48] In many of the studies, the combination vehicles were effective at inhibiting the growth of both HER2+ cancer cells and many multidrug resistant cancer cell lines.

While current delivery platforms are capable of delivering LAP and PTX in combination, their release rates can not be independently controlled. Further efficacy may be achieved by programmable delivery aimed at optimizing the sequence and ratio in which the drugs are administered. Previously, pretreatment with trastuzumab (which also inhibits the HER2 receptor) prior to PTX was more effective at initiating apoptosis in HER2+ cancer cells than the simultaneous exposure of the two agents.[49] It was postulated that a similar mechanistic advantage might also contribute to the combined LAP and PTX therapy. However, there is no way to manipulate the relative release rates of the drugs from the current delivery platforms. Therefore, we hypothesized that our pH responsive Janus nanoparticle delivery system would allow for the drugs to release at different rates and could result in a greater degree of synergy.

2.3. Free Drug Synergy

Using BT-474 cells as a representative cell line for HER2+ breast cancer, the activity of both LAP and PTX was individually determined for different drug exposure times (**Figure 3**A–D). In all cases, efficacy and individual drug IC_{50} values were determined at the 72 h timepoint. LAP (Figure 2A,B) and PTX (Figure 2C,D) were either incubated with the cells for the entire 72 h (blue line) or introduced for a shorter periods (red, 24 h and black, 4 h) while the remaining time the cells were incubated in drug-free media. The 72 h IC_{50} doses for LAP and PTX, when administered for the entire 72 h, were determined to be $85 \times 10^{-9} \pm 10 \times 10^{-9}$ and $14 \times 10^{-9} \pm 1 \times 10^{-9}$ M, respectively. Decreasing the exposure time of each drug from 72 to 24 h increased the IC_{50} dose 3x and 6x for LAP and PTX, respectively. On the contrary, delaying the exposure of LAP and PTX for 24 h increased the IC_{50} dose ≈3x for both drugs.

After identifying the relative activity of each drug on its own, cellular proliferation was measured following exposure to combinations of LAP and PTX. Exploring a range of molar ratios, it was found that a 3:1 (LAP:PTX) molar ratio provided the greatest synergistic effect. Treating cells with that same fixed molar ratio, (3:1, LAP:PTX), near the IC_{50} of each drug, the cells were exposed to different schedules of drugs (Figure 3E). Given the cell viability after exposure to the individual drugs compared

© 2020 Wiley-VCH GmbH

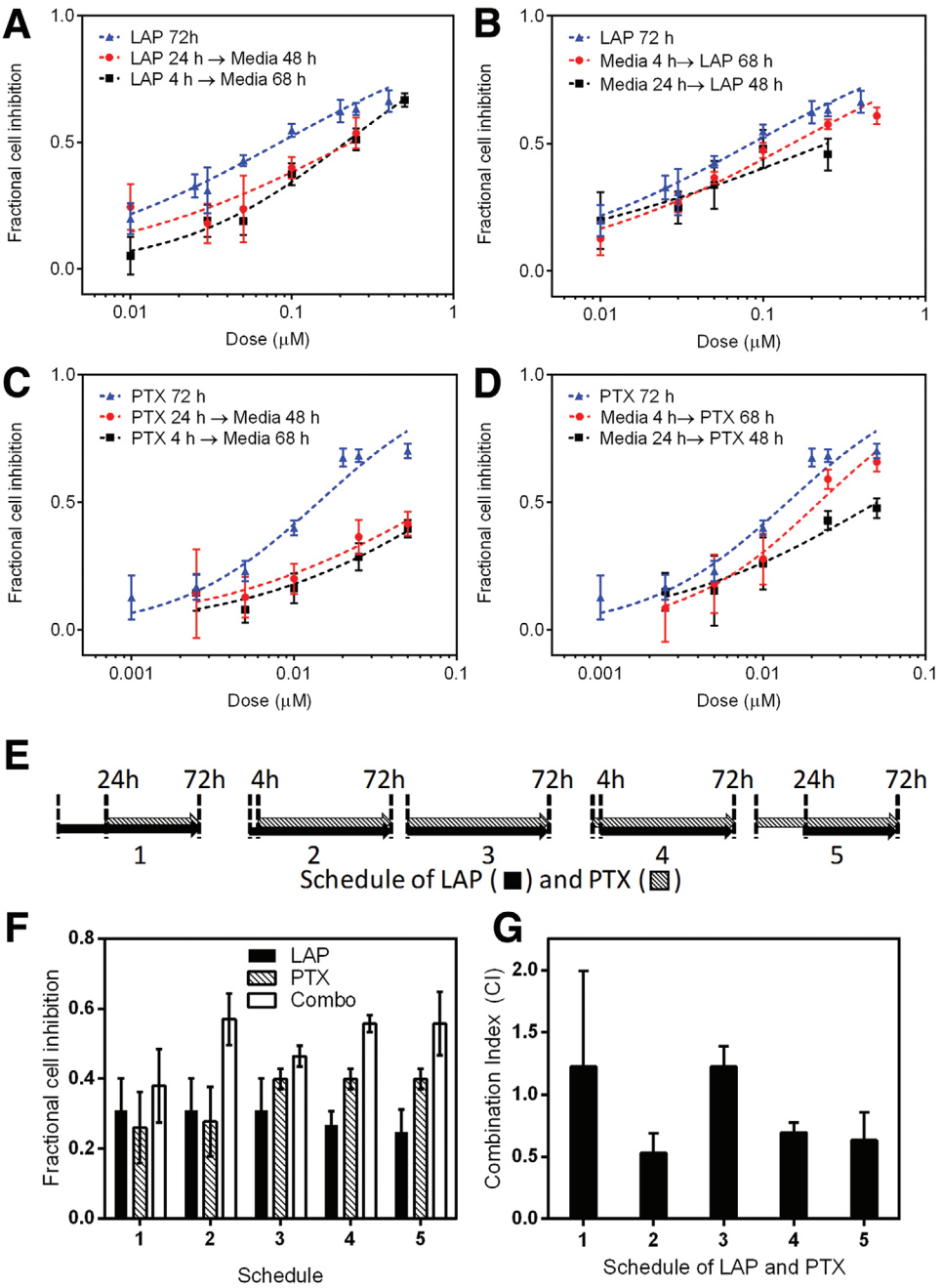

Figure 3. Free-drug cell inhibition and synergistic drug combination studies in HER2+ breast cancer cells. A–D) Fractional cell inhibition and relevant dose response curves for BT-474 cells after exposure to A) LAP → media, B) media → LAP, C) PTX → media, and D) media → PTX. Cell viability was assessed at 72 h for each schedule. Points are experimental data and lines are best fit median effect model. Error bars represent 95% CI ($n \geq 12$ wells). E) 72 h incubation schedule of LAP and PTX combinations. F) Fractional cell inhibition as a function of different LAP (0.03 μM) and PTX (0.01 μM) schedules evaluated with MTT assay. Results are shown as mean ± 95% CI ($n \geq 6$ wells). G) Combination index as a function of schedule. Error bars represent 95% CI ($n \geq 6$ wells).

to the combination treatments (Figure 3F), it was determined that giving LAP 4 h prior to PTX (Schedule 2) is significantly more effective than giving the two drugs simultaneously (Schedule 3) (Figure 3F). This holds true whether LAP is present after PTX exposure or whether extracellular LAP is removed after PTX exposure. In addition, it is also synergistic if PTX is given prior to LAP (Schedules 4 and 5); however, this combination is less active than the reverse schedule where LAP was delivered first.

Using the optimal schedule of LAP (4 h) → PTX/LAP (68 h), the effect of molar ratio on synergy between the two drugs was studied. With a PTX dose below the IC_{50} (0.10×10^{-6} M), molar ratios of LAP:PTX greater than 1 are synergistic (combination index, CI < 1) (Figure S4, Supporting Information). However, as

© 2020 Wiley-VCH GmbH

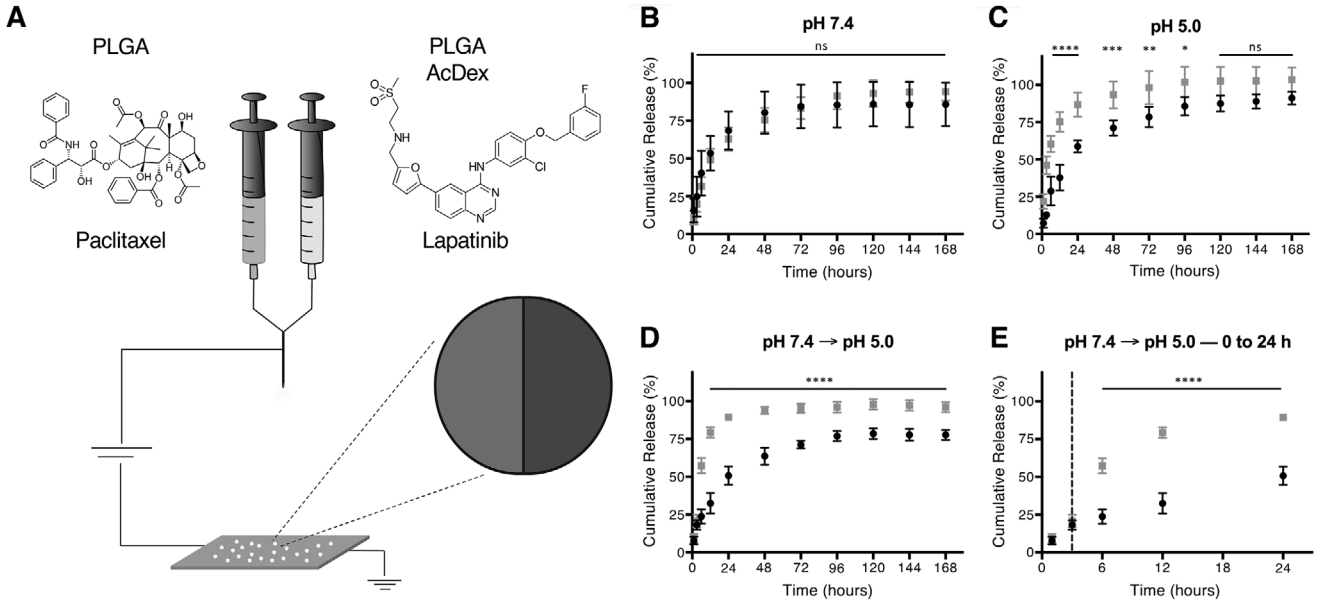

Figure 4. Synthesis and characterization of programmable nanoparticles via EHD cojetting. A) Fabrication of pH responsive, dual drug-loaded particles. PTX and LAP were encapsulated within distinct PLGA and pH responsive PLGA/AcDex compartments. B–D) Controlled release of PTX and LAP from PLGA and AcDex/PLGA nanoparticle compartments, respectively. B) Extended and uniform cumulative release is observed at physiological pH, 7.4 with no statistically significant difference observed at any time point ($p > 0.05$). C) Release under acidic conditions indicate a pH dependency on release kinetics with rapid degradation and release of LAP from the AcDex/PLGA compartment. A statistically significant difference in cumulative release is observed during the intermediate phase (6 h $< t <$ 120 h) of combined drug release. D) A change in pH at $t = 3$ h from 7.4 (physiological, circulation) to 5.0 (acidic, intracellular), designed to simulate in vivo systemic delivery, further demonstrates pH dependency on release kinetics. All timepoints greater than 6 h show significant differences comparing PTX and LAP cumulative release ($p < 0.0001$). E) A focused look at the first 24 h of (D), more clearly shows the significant departure of the combined release kinetics following the pH change at $t = 3$ h. Results are shown as mean ± SD. Statistical significance defined as $p < 0.05$ ($n = 6$ biological replicates; two-way ANOVA and Sidak's multiple comparisons tests; **** $p < 0.0001$, *** $p < 0.0005$, ** $p < 0.005$, * $p < 0.05$).

the dose of PTX is increased significantly above the IC_{50} (0.30×10^{-6} M), the synergy decreases compared to lower PTX doses. This is likely due to the fact that at this high concentration, PTX is already significantly potent as a single drug. Together, these data motivated the proposed design of loading and rapidly releasing LAP from the PLGA/AcDex compartment while complimenting it with a slow and sustained release of PTX from the PLGA compartment (**Figure 4**A).

2.4. Synthesis and Characterization of Drug-Loaded Nanoparticles

To characterize the release kinetics of each drug, a full release study was completed for the particles of interest. Again, LAP was encapsulated within the AcDex/PLGA compartment, designed to release quickly in response to acidic environments; meanwhile, PTX was encapsulated within the PLGA-only compartment with a goal of creating a delayed release relative to that of LAP. Following a similar approach to the release of dyes, three different conditions were evaluated, pH 7.4, pH 5.0, and a dynamic release condition consisting of a change of pH (at $t = 3$ h) from physiological to acidic conditions.

In all cases, it is observed that a significant release of drugs from the particles occurs within the first 72 h. In neutral conditions, an extended release of each drug is observed with no significant difference seen between the release profiles of the individual drugs (Figure 4B). However, it is evident that in acidic release conditions, LAP is preferentially released due to the rapid and selective degradation of the AcDex/PLGA compartment (Figure 4C). Furthermore, when the release buffer is exchanged at $t = 3$ h, a rapid burst release of LAP is observed compared to that of the PTX (Figure 4D). This is most clearly seen in the first 24 h, highlighted in Figure 4E.

2.5. Cancer Activity of Programmable Nanoparticles

A variety of bicompartmental nanoparticles were cojetted with LAP and PTX. Both LAP and PTX were loaded into bicompartmental nanoparticles by dissolving the drugs in the individual polymeric solutions. The drugs were loaded into different compartments to change the relative release rate of each drug (Table S1, Supporting Information). While each particle system was jetted with LAP and PTX concentrations to give final drug loadings of 2.7 and 5.5 wt%, respectively, approximately a fourfold lower drug loading remained after collecting, purifying, and washing each particle type, determined with high performance liquid chromatography-mass spectroscopy (HPLC-MS). Despite this, the approximate target 3:1 molar ratio of LAP:PTX was achieved in each of the final particle formulations with loading efficiencies ranging from 22% to 28%. Control particles were also made with just a single drug or no drug encapsulated to further investigate the advantage of dual-loaded bicompartmental

© 2020 Wiley-VCH GmbH

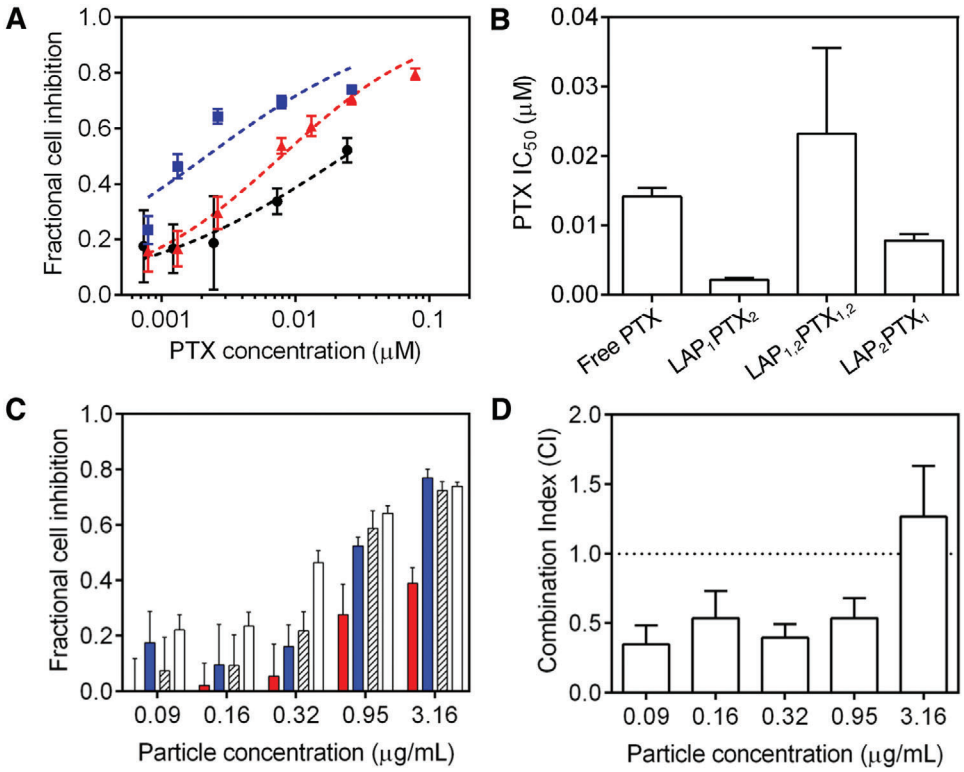

Figure 5. Cancer activity and synergism in HER2+ breast cancer cells. A) Fractional cell inhibition of BT-474 cells after 72 h exposure to the following bicompartmental particles: LAP_1PTX_2 (AcDEX/PLGA: LAP, PLGA: PTX, blue), $LAP_{1,2}PTX_{1,2}$ (AcDEX/PLGA: LAP + PTX, PLGA: LAP + PTX, black), and LAP_2PTX_1 (AcDEX/PLGA: PTX, PLGA: LAP, red). Points are experimental data and lines are best fit median effect model. B) PTX IC_{50} concentrations for each particle type. Error bars represent 95% CI ($n \geq 12$ wells). C) Fractional cell inhibition of BT-474 cells after 72 h exposure to the following bicompartmental particles: LAP_1 (AcDEX/PLGA: LAP, PLGA: blank, red), PTX_2 (AcDEX/PLGA:blank, PLGA:PTX, blue), LAP_1 + PTX_2 (black), and LAP_1PTX_2 (AcDEX/PLGA: LAP, PLGA: PTX, white). Results are shown as mean ± 95% CI (n ≧ 6 wells). D) Combination index for particle LAP_1PTX_2. Error bars represent 95% CI ($n \geq 6$ wells).

particles and possible toxicities associated with the polymers themselves. Particles, regardless of their drug content, were found to have an average size of ≈160 nm with low polydispersity in their dry state, similar to both unloaded and dye loaded particles previously synthesized.

Prior to determining the efficacy of the drug loaded particles at inhibiting cancer cell growth, the toxicity of the blank particles was determined on MDA-MB-231 (HER2−) and BT-474 (HER2+) cells (Figure S5, Supporting Information). Up to a particle concentration of 3 μg mL^{-1}, no toxicity was observed for the blank particles in either cell line. Higher particle concentrations were not evaluated because these particle concentrations were sufficiently high for toxicity testing in vitro with the drug loaded particles.

The activity of the different bicompartmental nanoparticle iterations (Table S1, Supporting Information) was evaluated on BT-474 cells (**Figure 5**B). Drug loadings of each formulation were determined by HPLC-MS and used to standardize all experimental groups to produce comparable data points for dose response curves allowing a direct comparison to be made between all particle types and previously conducted free drug studies. Bicompartmental particles which contained LAP in the AcDEX/PLGA compartment and PTX in the PLGA compartment (LAP_1PTX_2) induced the most cellular toxicity of the particles loaded with both drugs. Both particles which contained PTX and LAP in different compartments (LAP_1PTX_2 and LAP_2PTX_1) have a lower PTX IC_{50} ($4.3 \times 10^{-9} \pm 0.5 \times 10^{-9}$ and $6.6 \times 10^{-9} \pm 0.7 \times 10^{-9}$ M, respectively) than free PTX ($14 \times 10^{-9} \pm 1 \times 10^{-9}$ M). Interestingly, the particle system which contained both drugs in the AcDEX/PLGA compartment ($LAP_{1,2}PTX_{1,2}$) is not as potent as free PTX. All combination particle systems were significantly more potent than free LAP at the concentrations tested.

The cellular activity of the most potent nanoparticle (LAP_1PTX_2) was then compared to a physical mixture of single drug loaded particles with LAP and PTX in the AcDEX/PLGA and PLGA compartments, respectively. Again, HPLC-MS measured drug loadings informed the study to ensure equal dosing between the various experimental groups. The dual loaded particle (LAP_1PTX_2) was considerably more potent than both the PTX and LAP control particles (Figure 5C) which had similar drug loadings to the dual loaded particle. In addition, the dual loaded particle (LAP_1PTX_2) is much more effective at inhibiting BT-474 cell growth than a physical mixture of LAP and PTX control particles (LAP_1 and PTX_2) at similar drug concentration. Compared to the single drug loaded particles, the dual loaded particles are synergistic at inhibiting cell growth (CI < 0.5) for particle concentrations less than 1 μg mL^{-1} (Figure 5D).

© 2020 Wiley-VCH GmbH

The activity of the bicompartmental nanoparticles was also evaluated in triple negative breast cancer cells (MDA-MB-231). Because triple negative cells are HER2−, LAP is typically ineffective at inhibiting MDA-MB-231 growth. Using LAP concentrations which are relevant to the particle systems (up to 100×10^{-9} M), LAP does not inhibit any MDA-MB-231 growth. However, LAP has shown to enhance the activity of other cytotoxic drugs on HER2− cancer cells by inhibiting drug efflux pumps.[42,50]

Interestingly, both dual loaded particle systems are more active than the single loaded PTX particles against MDA-MB-231 cells, even though the single loaded LAP particles show no signs of toxicity (Figure S6, Supporting Information). The IC_{50} for the dual loaded particles LAP_1PTX_2 and $LAP_{1,2}PTX_{1,2}$ is 3x and 2x lower, respectively, than the single loaded PTX particles. In addition, the most toxic dual loaded particle (LAP_1PTX_2) has a significantly lower IC_{50} than free PTX (LAP_1PTX_2: $4.3 \times 10^{-9} \pm 0.6 \times 10^{-9}$ M, free PTX: $11 \times 10^{-9} \pm 2 \times 10^{-9}$ M). When tested in nontumorigenic mammary epithelial MCF 10a cells, lower IC_{50} values were found for all particle types compared to each of the breast cancer cells lines. The results follow a similar trend to free PTX in the various cell lines (Table S2, Supporting Information).

3. Discussion

LAP has been used in combination with many other chemotherapeutics in the clinic due to its ability to enhance tumor inhibition. In particular, the combination of LAP and PTX has proven to be an effective drug combination for treating late stage, metastatic breast cancer. Here, we show that the drug pair is synergistic at inhibiting the growth of HER2+ breast cancer cells if given in the correct sequence. We then demonstrate that we can synthesize programmable nanoparticles which are capable of controlling both the molar ratio of LAP and PTX and the relative release rate of each drug.

The HER2+ cell line BT-474 is responsive to both LAP and PTX with single drug IC_{50} values in the nM range; however, the combination of LAP and PTX is not synergistic, if the cells are exposed to both drugs simultaneously. If the schedule of drug administration is controlled, such that the one drug is exposed prior to the other drug, the combination becomes synergistic indicating a lower drug dose can be administered to achieve the same cellular growth inhibition. In free drug studies, synergy is the highest when LAP is given 4 h prior to PTX at a molar ratio of LAP:PTX of 3:1. For the optimal schedule, the CI is ≈0.5, indicating that a twofold lower dose of PTX can be given. It is evident that synergy between LAP and PTX is highly dependent upon both the schedule and molar ratio of LAP and PTX while treating BT-474 cells. This is consistent with a previous study which showed that trastuzumab can only enhance the activity of PTX on HER2+ cancer cells if the cells are exposed to trastuzumab first.[49]

The strong dependence of drug synergy on drug ratio and temporal schedule makes it difficult to translate an effective combination dosing regimen to the clinic due to the complicated pharmacokinetics. Various nanosized delivery vehicles have been synthesized to carry both LAP and PTX to ensure that cancer cells are exposed to the drugs simultaneously; however, drug release from these vehicles cannot be changed without changing the physical structure of the vehicle and/or drug loading process.[40,44–48,50] Here, we used EHD cojetting to synthesize Janus nanoparticles which enable us to manipulate the release rate and molar ratio of drug-loaded particles without drastically changing the drug loading technique and/or overall particle structure.

Bicompartmental nanoparticles were synthesized with one compartment containing AcDEX/PLGA and one compartment containing PLGA. The particles are less than 250 nm, ideal for surface modifications such as PEGylation or CD-47 conjugation facilitating extended particle circulation and accumulation in tumors with leaky vasculature following systemic administration. The Janus morphology of the nanoparticles was verified with super resolution microscopy, and each compartment degrades and releases their encapsulated cargo at a different rate. The AcDEX/PLGA compartment is pH responsive and degrades significantly faster in acidic pH than the PLGA compartment. It is expected that the drugs which are loaded into the AcDEX/PLGA compartment will be available to the cell faster than drugs loaded in the PLGA compartment, due to bulk polymer degradation in response to the acidic environment in the TME, endosomes, and lysosomes. Furthermore, while not shown here, AcDex degradation kinetics and composition of the AcDEX/PLGA compartment can also be manipulated to further control the relative release rate of each compartment.[32]

Both LAP and PTX could be loaded into either particle compartment, so dual loaded particles were synthesized varying which compartment each drug was loaded in. Particles which contained LAP in the AcDEX/PLGA compartment and PTX in the PLGA compartment were considerably more potent to BT-474 (HER2+) cells than the particles which contained both LAP and PTX in the AcDEX/PLGA compartment. This is consistent with the free drug data, which shows that exposing BT-474 cells to LAP prior to PTX is more synergistic than exposing the cells to both drugs concurrently. Furthermore, the dual-loaded particles were more potent than the combined delivery of single drug loaded particles at the same drug dose, demonstrating that synergy is maintained between PTX and LAP. Surprisingly, the dual drug loaded particles were also more potent to triple negative breast cancer cells (MDA-MB-231), even though the cells are unresponsive to LAP on its own. The enhanced activity is likely due to the inhibition of efflux drug pumps with LAP;[42,50] however, further research is required to explore this effect in detail.

The primary advantage of using dual drug loaded particles is that cells are exposed to the drug pair, regardless of how the individual free drugs distribute in the body. However, it is often advantageous to expose the cells to one drug prior to the other drug. Here, the therapeutic activity of dual loaded PTX/LAP particles could be manipulated in vitro by changing the relative release kinetics of the drug pair by changing which compartment the drugs were incorporated into and their bulk composition. The ability to manipulate individual drug release kinetics provides another adjustable parameter while designing combination drug particles. Previous studies have synthesized core–shell particles to release one drug relatively faster than another drug; however many of these systems rely on differences in drug hydrophobicity to load into different regions of the particle.[51–55] On the contrary, by using EHD cojetting, the relative release rate of PTX and LAP, and the resulting cellular toxicity, could easily be manipulated by changing reaction conditions and final particle architecture. This

© 2020 Wiley-VCH GmbH

observed control of release kinetics is not limited to this particular drug pair.

While the dual loaded particles containing LAP in the AcDEX/PLGA compartment were most effective at inhibiting cancer cell growth in vitro on BT-474 cells and MDA-MB-231 cells, this will not be true for all cell lines. Furthermore, other pairs of chemotherapeutic agents will demonstrate schedule-dependence, motivating the development of new delivery platforms capable of controlling the release rate of multiple therapeutics. Moving forward, the effect of drug release needs to be evaluated with respect to not only cancer cell activity in vitro but also healthy cell activity and in vivo efficacy. Regardless of the drug combination, the effect of drug schedule should be critically evaluated when designing a delivery vehicle to carry multiple agents.

4. Conclusions

Cancer therapy approaches continue to move toward the use of combination therapy in an attempt to maximize treatment efficacy and limit harmful off-target effects. Despite recent advances and the identification of promising drug combinations, effectively delivering these to the site of the tumor remains a challenge. The development of bicompartmental nanoparticles with distinct degradation profiles provides a method to control both the loading and release of multiple drugs from a single platform. Distinct to this approach is an ability to deliver the individual drugs in a temporally controlled manner in response to changes in pH. Through the encapsulation and controlled release of both surrogate small molecule dyes and two established chemotherapeutic drugs, it has been demonstrated that the release kinetics can be controlled and are dependent upon the bulk material properties of the discrete compartments rather than the chemical structure of the molecule being released. While demonstrated here in HER2+ breast cancer delivering LAP and PTX, the versatility of the EHD cojetting technology allows the concept of programmable nanoparticles to be extended to other drug combinations where dose and timing are found to be important factors to achieve synergistic effects. Future work aims to further evaluate this system in vivo, investigate targeting approaches for systemic delivery of the bicompartmental platform, and explore novel drug combinations where programmable delivery may increase therapeutic efficacy.

5. Experimental Section

Materials—Cells: MDA-MB-231, BT-474, Media: Hybricare, mammary epithelial cell growth medium (MEGM) kit, fetal bovine serum (FBS), penicillin-streptomycin

Materials—Drugs: Lapatinib free base (LC Laboratories), paclitaxel (LC Laboratories), ixapebilone

Materials—Reagents: 3-(4,5-dimethylthiazol-2-yl)-2,5-diphenyltetrazolium bromide (MTT) assay, phosphate buffered saline (PBS), PLGA 5004a (Corbion), deuterated water (D_2O, TCI America), dextran from Leuconostoc mesenteroides (64–76 kDa, Sigma), anhydrous dimethyl sulfoxide (DMSO, Sigma), pyridinium *p*-toluenesulfonate, 2-methoxypropene (Sigma), trimethylamine (TEA, Sigma), deuterated chloroform (Sigma), chloroform (Sigma), dimethylforamide (DMF, Sigma), acetonitrile (Sigma), hexadecyltrimethylammonium bromide (CTAB, Sigma), Tween 20 (Sigma), Coumarin 314 (Sigma), Rhodamine B (Sigma)

Cell Growth: All cells were grown in a humidified incubator at 37 °C and 5% CO_2. BT-474 cells were grown in Hybricare media supplemented with 10% FBS and 1% PS. MDA-MB-231 cells were grown in supplemented MEGM media.

Activity Assays: BT-474 and MDA-MB-231 cell suspensions (100 µL) were seeded in 96 well plates at concentrations of 1.1×10^4 and 1.0×10^4 cells per well, respectively. Cells were allowed to adhere overnight, and the media was replaced with drug or particle formulations the following day. Pure drug solutions were prepared from DMSO stocks of the drugs (1 mg mL^{-1} PTX and 1 mg mL^{-1} LAP). Particle formulations were prepared by suspending the lyophilized particles in PBS (≈0.1 mg mL^{-1}) with 0.01% Tween 20 and then dispersed with ultrasonication.

After cells were incubated with drugs for 72 h, unless specified otherwise, the drug formulations were replaced with MTT reagent (0.5 mg mL^{-1} in media). Following 4 h incubation, the MTT solution was aspirated and DMSO was added to each of the wells. The plates were shaken for 30 min and the absorbance of each well was read at 570 nm (Tecan Plate Reader). Dose response curves were calculated similarly to previous reports. Synergy between combination treatments were calculated using the combination index first published by Chou and Talalay.[56]

Synthesis of Acetylated Dextran: Acetylated dextran was synthesized according to a modified version of the protocol developed by Fréchet for the acetalation of low molecular weight dextrans.[29] Briefly, 1 g of dextran (64–76 kDa) was dissolved in 50 mL of anhydrous DMSO. Once, completely dissolved, 25 mg of pyridinium *p*-toluenesulfonate was introduced, followed by 5 mL of 2-methoxypropene, added dropwise. The reaction vessel was purged with dry N_2 and stirred for 3 h under positive pressure at room temperature. Acetylated dextran was precipitated out of solution by combining the reaction mixture with 200 mL of distilled H_2O (+1 v/v% TEA). The product was washed several times with DI water via alternating centrifugation and resuspension cycles. The final product was lyophilized to remove any water, yielding a dry, white powder.

Polymer Characterization: Synthesized acetylated dextran was characterized via proton NMR spectroscopy to confirm polymer structure and characterize acyclic versus cyclic hydroxyl protection. To determine the degree of protection, protected dextran was hydrolyzed in D_2O with a small addition of DCl to acidify the solution. Proton NMR spectra was collected using a Varian 400 MHz (University of Michigan (UM), Chemistry NMR Core) instrument. The resulting ^{1}H NMR spectra was used to calculate the fraction of hydroxyl groups protected through the reaction and estimate the ratio of acyclic versus cyclic acetal protecting groups using Equations (1) and (2), respectively.

$$\left[\frac{\left(\left(\frac{\text{MeOH}}{3}\right)+\left(\frac{\text{Acetone} - (2)(\text{MeOH})}{3}\right)\right)}{300}\right](100\%) \quad (1)$$

$$\text{MeOH} : \text{Acetone} - (2)\,(\text{MeOH}) \quad (2)$$

Validation of the protected acetylated dextran and its degradation in acidic conditions was validated through the controlled degradation of synthesized particles. Bicompartmental nanoparticles consisting of two compartments, one PLGA only, and a second, a PLGA/AcDex blend, were synthesized via EHD cojetting. The particles were dried under vacuum to remove any residual solvent and suspended in either neutral pH conditions (PBS + 0.1% Tween 20, pH 7.4) or acidic buffer (sodium acetate-acetic acid buffered solution + 0.1% Tween 20, pH 5.0). Particles were incubated at 37 °C for predetermined periods of time. At the end of the incubation period, nanoparticles were washed three times with PBS followed by five ultrapure water washes to remove any residual salts. Final nanoparticle solutions were spin coated onto silicon wafers and imaged via scanning electron microscopy.

Particle Synthesis: All carrier formulations were fabricated using electrohydrodyamic (EHD) cojetting as previously described.[16,17,27] Briefly, PLGA compartments consisted of a 7.0 w/v% PLGA in a

© 2020 Wiley-VCH GmbH

70:30 v/v $CHCl_3$:DMF solution. AcDex/PLGA compartments consisted of a 2.5 w/v% PLGA and 4.5 w/v% acetylated dextran in a 70:30 v/v $CHCl_3$:DMF solution. In each case, a small addition (2 w/v%) of CTAB was added to act as a surfactant to control for final particle size. When encapsulating chemotherapeutic drug into the particle system, drugs were first dissolved in DMSO at concentrations of 100 mg mL^{-1} and then diluted to target concentrations, relative to base polymer in $CHCl_3$. Bicompartmental particles were fabricated by flowing solutions for each of the two compartments in a side-by-side arrangement and cojetted at a total flow rate of 0.2 mL h^{-1}, 30 cm needle to collector distance, and 9.5–11.0 kV applied electrical potential. All cojetted particles were dried under vacuum for 3 weeks to ensure residual solvent was completely removed before their further use in future experiments.

Particle Characterization: Particles were characterized in both their dry and hydrated states to determine size, particle morphology and structure, and drug loading efficiencies. Particles were collected on small silicon wafers placed on the collection platform, dried under vacuum, and sputter coated with a thin (<10 nm) layer of conductive gold prior to imaging according to previously developed methods. SEM imaging was completed with an FEI NOVA 200 Nanolab Scanning Electron Microscopy-Focused Ion Beam (SEM-FIB) instrument (UM, $(MC)^2$ Imaging Core). Particle size distribution was determined by manually measuring particle diameter using ImageJ software ($n \geq 300$). Particles with dyes loaded into each compartment, were collected on glass cover slides, dried under vacuum and mounted in ProLong Diamond Antifade Mountant, and imaged using super-resolution SIM with a Ziess ELYRA microscope (UM, Biointerfaces Optical Imagine and Analysis Lab). All samples were imaged following a standard Zeiss developed, channel alignment protocol to eliminate alignment artifacts when investigating Bicompartmental particle nature. DLS was performed using a Malvern Zetasizer Nano ZSP (UM, Biointerfaces Nanotechnicum), following particle collection and purification in PBS (+0.1% Tween 20).

Particle Loading and Release: To determine loading and loading efficiency, particles were fabricated incorporating Coumarin 314 into the PLGA compartment and Rhodamine B into the AcDex/PLGA compartment. Known particle masses were collected and dissolved in chloroform. The resulting solutions were examined using a Horiba FluoroMax-3 Fluorometer with excitation/emission wavelengths of 436/485 and 543/576 nm, respectively. Results were compared to previously generated calibration curves to determine total dye loading.

A similar approach was used to determine drug loading for all drug-loaded particle variations. Particles were dried under vacuum as previously described and then dissolved in chloroform. Resulting solutions were analyzed for drug concentrations using an Agilent Quadrupole Time-of-Flight (Q-TOF) HPLC-MS instrument (UM, Chemistry Mass Spec Lab). Previously generated calibration curves were used to determine total drug loading, loading efficiency, and relative molar ratios in particles that encapsulated both compounds.

Release kinetics were determined via dialysis. In both dye and drug release experiments, known particle masses were collected and suspended in 5 mL of release media. PBS was used as neutral release media, while a sodium acetate-acetic acid buffered solution, adjusted to pH 5.0, was used for acidic release conditions. Particle solutions were placed within a Float-a-Lyzer device (100 kDa molecular weight cut-off, Spectrum Labs) and submerged in an additional 40 mL of equivalent release media in 50 mL conical vials. The vials were incubated at 37 °C. At predetermined times, the dialysis device was transferred to a new conical vial filled with prewarmed, fresh release media.

Samples from preliminary dye release experiments were measured as described above using the Horiba FluoroMax-3 Fluorometer. Samples from drug release experiments were measured as described above using the Agilent Q-TOF HPLC-MS instrument. In each, case a previously generated calibration curve was used to quantify cumulative release.

Statistical Analysis: All values are expressed as mean ± standard deviation ($n \geq 3$ biological replicates). Fractional cell inhibition and dose response curves were fit using nonlinear fits and display error bars of 95% confidence intervals. Statistical analysis and nonlinear median effect model fits were performed using GraphPad Prism 7. For normally distributed data sets, two-way Analysis of Variance (ANOVA) testing followed by Sidak post hoc tests were used to test statistical difference between measurements; *p*-values less than 0.05 were considered significant.

Supporting Information

Supporting Information is available from the Wiley Online Library or from the author.

Acknowledgements

The authors thank S. Rahmani and L. Solario for training and guidance. This work was partly supported by the Defense Threat Reduction Agency Grant HDTRA1-15-1-0045 and National Science Foundation (NSF) grant DMR-0320740. The authors acknowledge technical support from the Michigan Center for Materials Characterization.

Data and Materials Availability

All data supporting the findings of this study are available in the manuscript or the supplementary materials.

Conflict of Interest

The authors declare no conflict of interest.

Author Contributions

D.R.V. and J.V.G. contributed equally to this work. S.M. and J.L. proposed and supervised the project. D.R.V. and J.V.G. conducted experiments with assistance from A.B. and M.A.C. D.R.V., J.V.G., S.M., and J.L. analyzed the data and wrote the paper with input from all co-authors.

Keywords

cancer, combination therapy, drug delivery, nanomedicine, nanoparticles

Received: April 7, 2020
Revised: June 23, 2020
Published online: September 21, 2020

[1] R. B. Mokhtari, T. S. Homayouni, N. Baluch, E. Morgatskaya, S. Kumar, B. Das, H. Yeger, *Oncotarget* **2017**, *8*, 38022.
[2] X. Xu, W. Ho, X. Zhang, N. Bertrand, O. Farokhzad, *Trends Mol. Med.* **2015**, *21*, 223.
[3] J. B. Fitzgerald, B. Schoeberl, U. B. Nielsen, P. K. Sorger, *Nat. Chem. Biol.* **2006**, *2*, 458.
[4] J. Jia, F. Zhu, X. Ma, Z. W. Cao, Y. X. Li, Y. Z. Chen, *Nat. Rev. Drug Discovery* **2009**, *8*, 111.
[5] Z. Sheng, Y. Sun, Z. Yin, K. Tang, Z. Cao, *Briefings Bioinf.* **2017**, *19*, 1172.
[6] L. D. Mayer, A. S. Janoff, *Mol. Interventions* **2007**, *7*, 216.
[7] P. Nowak-Sliwinska, A. Weiss, X. Ding, P. J. Dyson, H. Van Den Bergh, A. W. Griffioen, C. M. Ho, *Nat. Protoc.* **2016**, *11*, 302.
[8] S. Y. Qin, Y. J. Cheng, Q. Lei, A. Q. Zhang, X. Z. Zhang, *Biomaterials* **2018**, *171*, 178.

 © 2020 Wiley-VCH GmbH

[9] K. A. Ryall, A. C. Tan, *J. Cheminf.* **2015**, *7*, 7.
[10] C. M. J. Hu, L. Zhang, *Biochem. Pharmacol.* **2012**, *83*, 1104.
[11] T. Patel, J. Zhou, J. M. Piepmeier, W. M. Saltzman, *Adv. Drug Delivery Rev.* **2012**, *64*, 701.
[12] S. Stolnik, L. Illum, S. S. Davis, *Adv. Drug Delivery Rev.* **2012**, *64*, 290.
[13] E. M. Pridgen, R. Langer, O. C. Farokhzad, *Nanomedicine* **2007**, *2*, 669.
[14] K. J. Lee, J. Yoon, J. Lahann, *Curr. Opin. Colloid Interface Sci.* **2011**, *16*, 195.
[15] J. H. Jordahl, S. Ramcharan, J. V. Gregory, J. Lahann, *Macromol. Rapid Commun.* **2017**, *38*, 1600437.
[16] S. Rahmani, A. M. Ross, T. H. Park, H. Durmaz, A. F. Dishman, D. M. Prieskorn, N. Jones, R. A. Altschuler, J. Lahann, *Adv. Healthcare Mater.* **2016**, *5*, 94.
[17] S. Rahmani, T. H. Park, A. F. Dishman, J. Lahann, *J. Controlled Release* **2013**, *172*, 239.
[18] A. C. Misra, S. Bhaskar, N. Clay, J. Lahann, *Adv. Mater.* **2012**, *24*, 3850.
[19] J. V. Gregory, P. Kadiyala, R. Doherty, M. Cadena, S. Habeel, E. Ruoslahti, P. R. Lowenstein, M. G. Castro, J. Lahann, **2019**, *2020*, 862581.
[20] M. S. Strozyk, D. J. de Aberasturi, J. V Gregory, M. Brust, J. Lahann, L. M. Liz-marzán, *Adv. Funct. Mater.* **2017**, *27*, 1701626.
[21] S. Rahmani, C. H. Villa, A. F. Dishman, M. E. Grabowski, D. C. Pan, H. Durmaz, A. C. Misra, L. Colón-Meléndez, M. J. Solomon, V. R. Muzykantov, J. Lahann, *J. Drug Targeting* **2015**, *23*, 750.
[22] A. C. Misra, K. E. Luker, H. Durmaz, G. D. Luker, J. Lahann, *Biomacromolecules* **2015**, *16*, 2412.
[23] S. Rahmani, S. Ashraf, R. Hartmann, A. F. Dishman, M. V. Zyuzin, C. K. J. Yu, W. J. Parak, J. Lahann, *Bioeng. Transl. Med.* **2016**, *1*, 82.
[24] Y. Qie, H. Yuan, C. A. Von Roemeling, Y. Chen, X. Liu, K. D. Shih, J. A. Knight, H. W. Tun, R. E. Wharen, W. Jiang, B. Kim, *Sci. Rep.* **2016**, *6*, 1.
[25] P. L. Rodriguez, T. Harada, D. A. Christian, D. A. Pantano, R. K. Tsai, D. E. Discher, *Science* **2013**, *339*, 971.
[26] J. S. Brenner, D. C. Pan, J. W. Myerson, O. A. Marcos-contreras, C. H. Villa, P. Patel, H. Hekierski, S. Chatterjee, J. Tao, H. Parhiz, K. Bhamidipati, T. G. Uhler, E. D. Hood, R. Y. Kiseleva, V. S. Shuvaev, T. Shuvaeva, M. Khoshnejad, I. Johnston, J. V. Gregory, J. Lahann, T. Wang, E. Cantu, W. M. Armstead, S. Mitragotri, V. Muzykantov, *Nat. Commun.* **2018**, *9*, 2684.
[27] T. H. Park, T. W. Eyster, J. M. Lumley, S. Hwang, K. J. Lee, A. Misra, S. Rahmani, J. Lahann, *Small* **2013**, *9*, 3051.
[28] S. Hwang, J. Lahann, *Macromol. Rapid Commun.* **2012**, *33*, 1178.
[29] E. M. Bachelder, T. T. Beaudette, K. E. Broaders, J. Dashe, J. M. J. Fréchet, *J. Am. Chem. Soc.* **2008**, *130*, 10494.
[30] H. M. Borteh, M. D. Gallovic, S. Sharma, K. J. Peine, S. Miao, D. J. Brackman, K. Gregg, Y. Xu, X. Guo, J. Guan, E. M. Bachelder, K. M. Ainslie, *Langmuir* **2013**, *29*, 7957.
[31] T.-H. Park, T. W. Eyster, J. M. Lumley, S. Hwang, K. J. Lee, A. Misra, S. Rahmani, J. Lahann, *Small* **2013**, *9*, 3051.
[32] K. E. Broaders, J. A. Cohen, T. T. Beaudette, E. M. Bachelder, J. M. J. Fréchet, *Proc. Natl. Acad. Sci. U. S. A.* **2009**, *106*, 5497.
[33] D. A. Yardley, L. Hart, L. Bosserman, M. N. Salleh, D. M. Waterhouse, M. K. Hagan, P. Richards, M. L. Desilvio, J. M. Mahoney, Y. Nagarwala, *Breast Cancer Res. Treat.* **2013**, *137*, 457.
[34] A. Di Leo, H. L. Gomez, Z. Aziz, Z. Zvirbule, J. Bines, M. C. Arbushites, S. F. Guerrera, M. Koehler, C. Oliva, S. H. Stein, L. S. Williams, J. Dering, R. S. Finn, M. F. Press, *J. Clin. Oncol.* **2008**, *26*, 5544.
[35] N. M. Iyengar, M. N. Fornier, S. M. Sugarman, M. Theodoulou, T. A. Troso-Sandoval, G. M. D'Andrea, P. R. Drullinsky, D. Gajria, S. B. Goldfarb, E. A. Comen, D. E. Lake, S. Modi, T. A. Traina, M. E. Lacouture, M. F. Chen, S. Patil, J. Baselga, L. Norton, C. A. Hudis, C. T. Dang, *Clin. Breast Cancer* **2016**, *16*, 87.
[36] R. S. Finn, M. F. Press, J. Dering, M. Arbushites, M. Koehler, C. Oliva, L. S. Williams, A. Di Leo, *J. Clin. Oncol.* **2009**, *27*, 3908.
[37] J. Baselga, I. Bradbury, H. Eidtmann, S. Di Cosimo, E. De Azambuja, C. Aura, H. Gómez, P. Dinh, K. Fauria, V. Van Dooren, G. Aktan, A. Goldhirsch, T.-W. Chang, Z. Horváth, M. Coccia-Portugal, J. Domont, L.-M. Tseng, G. Kunz, J. H. Sohn, V. Semiglazov, G. Lerzo, M. Palacova, V. Probachai, L. Pusztai, M. Untch, R. D. Gelber, M. Piccart-Gebhart, *Lancet* **2012**, *379*, 633.
[38] R. Butti, S. Das, V. P. Gunasekaran, A. S. Yadav, D. Kumar, G. C. Kundu, *Mol. Cancer* **2018**, *17*, 34.
[39] M. Vouri, S. Hafizi, *Cancer Res.* **2017**, *77*, 2775.
[40] Y. Wei, S. Xu, F. Wang, A. Zou, S. Zhang, Y. Xiong, S. Cao, Q. Zhang, Y. Wang, X. Jiang, *J. Pharm. Sci.* **2015**, *104*, 165.
[41] A. J. Chien, J. A. Illi, A. H. Ko, W. M. Korn, L. Fong, L. Chen, M. Kashani-Sabet, C. J. Ryan, J. E. Rosenberg, S. Dubey, E. J. Small, T. M. Jahan, N. M. Hylton, B. M. Yeh, Y. Huang, K. M. Koch, M. M. Moasser, *Clin. Cancer Res.* **2009**, *15*, 5569.
[42] J. Perry, E. Ghazaly, C. Kitromilidou, E. H. McGrowder, S. Joel, T. Powles, *Mol. Cancer Ther.* **2010**, *9*, 3322.
[43] F. Li, M. Danquah, S. Singh, H. Wu, R. Mahato, *Drug Delivery Transl. Res.* **2011**, *1*, 420.
[44] P. D. Kelishady, E. Saadat, F. Ravar, H. Akbari, F. Dorkoosh, *Pharm. Dev. Technol.* **2015**, *20*, 1009.
[45] P. Dehghankelishadi, E. Saadat, F. Ravar, M. Safavi, M. Pordeli, M. Gholami, F. A. Dorkoosh, *Drug Dev. Ind. Pharm.* **2017**, *43*, 390.
[46] F. Ravar, E. Saadat, P. D. Kelishadi, F. A. Dorkoosh, *J. Liposome Res.* **2016**, *26*, 175.
[47] H. Hu, Z. Lin, B. He, W. Dai, X. Wang, J. Wang, X. Zhang, H. Zhang, Q. Zhang, *J. Controlled Release* **2015**, *220*, 189.
[48] D. Vergara, C. Bellomo, X. Zhang, V. Vergaro, A. Tinelli, V. Lorusso, R. Rinaldi, Y. M. Lvov, S. Leporatti, M. Maffia, *Nanomedicine* **2012**, *8*, 891.
[49] S. Lee, W. Yang, K.-H. Lan, S. Sellappan, K. Klos, G. Hortobagyi, M.-C. Hung, D. Yu, *Cancer Res.* **2002**, *62*, 5703.
[50] Y. S. Kwon, S. Y. Chun, K. S. Nam, S. Kim, *Oncol. Rep.* **2015**, *34*, 884.
[51] S. Sengupta, D. Eavarone, I. Capila, G. Zhao, N. Watson, T. Kiziltepe, R. Sasisekharan, *Nature* **2005**, *436*, 568.
[52] Z. J. Deng, S. W. Morton, E. Ben-Akiva, E. C. Dreaden, K. E. Shopsowitz, P. T. Hammond, *ACS Nano* **2013**, *7*, 9571.
[53] Z. Wang, P. C. Ho, *Biomaterials* **2010**, *31*, 7115.
[54] S. W. Morton, M. J. Lee, Z. J. Deng, E. C. Dreaden, E. Siouve, K. E. Shopsowitz, N. J. Shah, M. B. Yaffe, P. T. Hammond, *Sci. Signaling* **2014**, *7*, ra44.
[55] Y. He, Z. Su, L. Xue, H. Xu, C. Zhang, *J. Controlled Release* **2016**, *229*, 80.
[56] T. C. Chou, P. Talalay, *Adv. Enzyme Regul.* **1984**, *22*, 27.

© 2020 Wiley-VCH GmbH